

# Measurement of the longitudinal polarization of the top quark in top-antitop events with the ATLAS experiment.

Samuel Hamilton for the ATLAS Collaboration

Tufts University, Medford MA, United States of America

DOI: <http://dx.doi.org/10.3204/DESY-PROC-2014-02/56>

In the Standard Model (SM), top-antitop quark pair production ( $t\bar{t}$ ) is generated from both strong and weak interactions. At the Large Hadron Collider (LHC), the strong interaction is the dominant mechanism for producing top-antitop pairs. Parity conservation in the strong production of  $t\bar{t}$  renders un-polarized top quarks, meanwhile, parity-violating weak interactions generate a negligible contribution to the polarization [8]. The anomalous forward-backward asymmetry ( $A_{FB}$ ) results from the Tevatron experiments, D0 [9, 10] and CDF [11], have motivated theorists to explain the result using Beyond the Standard Model (BSM) mechanisms, such as axi-gluons, which produce non-zero longitudinal polarization of top quarks in top-antitop production [12, 13, 14]. The measurement of the longitudinal polarization of the top quark may be used as a check for the SM and as a way to probe the existence of BSM physics given the discrepancy between the SM and BSM predictions.

The analysis presented in this article measures the longitudinal polarization of the top quark in  $t\bar{t}$  production using the single lepton channel. In addition, the single lepton channel and dilepton channel are used to produce a combined measurement.

With a lifetime of  $3.29 \times 10^{-25}$  s [15], the top quark decays before hadronization can occur, allowing the spin information of the top quark to be accessed through its decay products. By utilizing this property of the top quark, its longitudinal polarization can be determined by analyzing the angular distribution of its final state decay products. The distribution of the polar angle,  $\theta_i$ , of each of the top quark's final state decay products, labeled by  $i$ , is given by

$$W(\cos\theta_i) = \frac{1}{2}(1 + \alpha_i P \cos\theta_i), \quad (1)$$

where  $P$  represents the degree of polarization along the chosen quantization axis and  $\alpha_i$  is the spin-analyzing power of the final state decay product [16, 17], which is a measure of the sensitivity of the daughter particle to the parent particle's spin state. Table 1 shows the tree level values of the spin-analyzing power for the final state particles of the top decay. For this analysis, the helicity basis is used, where the parent top quark's momentum direction in the  $t\bar{t}$

$\alpha_i$	Particle Type
1.0	Charged Lepton
1.0	Down and Strange Quarks
-0.4	b Quark
-0.3	Neutrino
-0.3	Up Type Quark

Table 1: Predicted tree level values of the spin-analyzing power,  $\alpha_i$ , for the top quark final state decay products.

center-of-mass frame is chosen as the quantization axis. Due to its  $\alpha_i$  value being 1, which gives it maximal sensitivity to the top quark's spin state, the charged lepton is utilized in this analysis to determine the longitudinal polarization of the top quark. The polar angle of the charged lepton,  $\theta_\ell$ , is determined by measuring the angle between the quantization axis and the charged lepton's momentum direction in its parent top quark's rest frame, as depicted in Figure 1. Templates of  $\cos\theta_\ell$ , which require  $t\bar{t}$  event reconstruction, are produced and fit to the data using a binned maximum likelihood fit. Results for the single lepton and combined fits are quoted as the product of  $\alpha_i$  and  $P$ .

The full 2011 dataset of proton-proton ( $pp$ ) collisions collected by the ATLAS detector [18] at a center-of-mass energy of  $\sqrt{s} = 7$  TeV, corresponding to an integrated luminosity of  $4.7 \text{ fb}^{-1}$ , is used for this analysis [19]. The single lepton channels considered for this analysis are the electron and muon channels. Selection cuts on event and object kinematics are performed to enhance the signal to background ratio for  $t\bar{t}$  events. The cuts used in this analysis are as follows: exactly one high- $p_T$  isolated electron or muon, at least four jets; with at least one  $b$ -tagged, large missing transverse energy from the neutrino, and a large transverse mass of the leptonically decaying  $W$ -boson, defined as

$$m_T = \sqrt{2p_T^\ell E_T^{\text{miss}} [1 - \cos(\phi^\ell - \phi(E_T^{\text{miss}}))]}, \quad (2)$$

where  $p_T^\ell$  is the transverse momentum of the charged lepton,  $E_T^{\text{miss}}$  is the missing transverse energy of the event,  $\phi^\ell$  is the azimuthal angle of the charged lepton, and  $\phi(E_T^{\text{miss}})$  is the azimuthal angle of the missing transverse energy. Monte Carlo (MC) simulated samples are used to determine the signal and background contributions, with the exception of the non-prompt(NP)/fake lepton contribution arising from QCD multi-jet events. The  $t\bar{t}$  signal MC was simulated using the next-to-leading order (NLO) MC@NLO 3.41 [7] generator with the NLO parton density function (PDF) set CT10 [6], assuming a top mass of 172.5 GeV. Parton showering is modeled with HERWIG 6.510 [5] and the underlying event is generated using JIMMY 4.31 [4]. Single top events were simulated using the MC@NLO generator for the  $Wt$  and  $s$ -channel, while the ACERMC [2] generator was used for the  $t$ -channel. Diboson ( $WW, WZ, ZZ$ ) events were simulated using the HERWIG generator. The production of  $W$  and  $Z$  bosons in association with jets were simulated using the ALPGEN [1] generator interfaced with HERWIG and JIMMY. The shapes of the kinematic distributions produced from the  $W$ +jets background are taken from the MC, however, the overall normalization of the events is scaled using the most recent ATLAS measurement of the cross section of this process [20]. The NP/fake lepton contribution is estimated using a data driven matrix method based on the ratio of jets passing loose lepton selection to those passing tight lepton selection [21, 22]. Table 2 shows the expected signal and background yields compared to data, after selection, for both of the single lepton channels.

The four momentum of both the top and antitop are needed in order to determine the quantization axis for the calculation  $\cos\theta_\ell$ , requiring a full reconstruction of the  $t\bar{t}$  system. A kinematic likelihood fit, which utilizes  $b$ -tagging information, is employed to determine the longitudinal momentum of the neutrino and to assign the selected jets to the top (antitop)

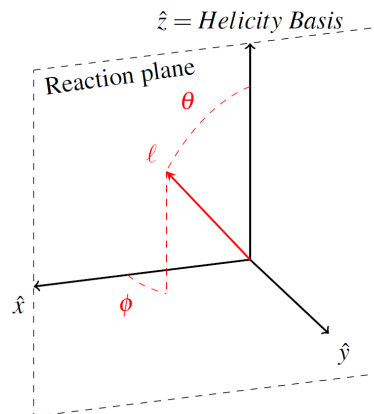


Figure 1: The Helicity Basis.

Table 2: Expected signal and background rounded yields compared to data for each of the single lepton channels considered. The total systematic and statistical uncertainties are reported.

Source	$e$ +jets	$\mu$ +jets
$t\bar{t}$	16200	26500
Background	5100	9400
Total	21300	35900
Uncertainty	$\pm 1300$	$\pm 1700$
Data	21956	37919

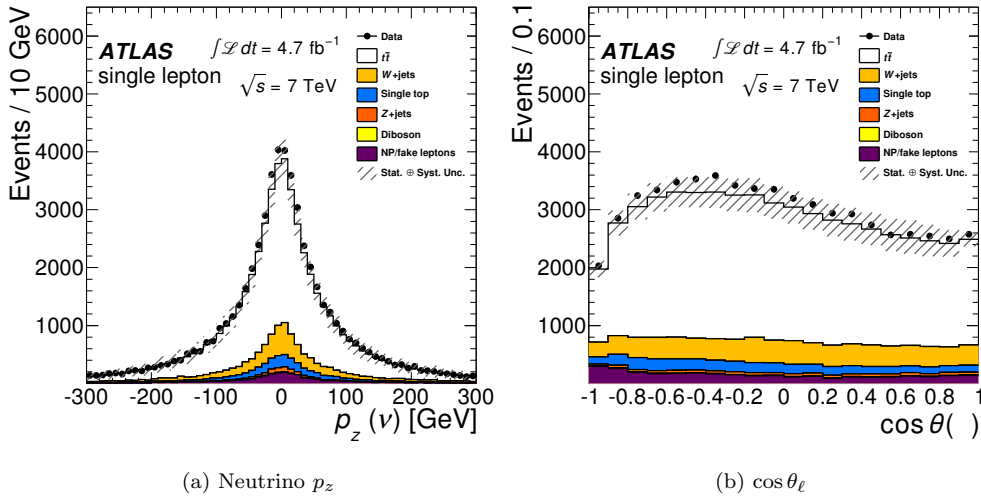


Figure 2: Comparison of the data to expectation based on MC and data driven predictions. The hatched error bands are formed from the statistical and systematic uncertainties.

decay [23]. Figure 2 depicts the performance of the kinematic fitter by displaying the data to expectation agreement after reconstruction for the neutrino  $p_z$  and  $\cos \theta_\ell$ .

After event reconstruction is performed, templates of  $\cos \theta_\ell$  for signal and background are produced and then fit to the data. The MC available for this analysis lacks polarized top quarks, requiring that the signal MC be reweighted to induce longitudinal polarization. Each MC signal event is reweighted based on the double differential cross section given by [24]

$$\frac{1}{\sigma} \frac{d\sigma}{d \cos \theta_1 d \cos \theta_2} = \frac{1}{4} (1 + \alpha_1 P_1 \cos \theta_1 + \alpha_2 P_2 \cos \theta_2 - C \cos \theta_1 \cos \theta_2), \quad (3)$$

where  $\alpha_1 P_1$  ( $\alpha_2 P_2$ ) corresponds to the spin-analyzing power of one of the final state decay products of the top (antitop) quark times the longitudinal polarization of the top (antitop) quark and  $C$  represents the  $t\bar{t}$  spin correlation. The angle  $\theta_1$  ( $\theta_2$ ) corresponds to the polar angle of the final state decay product used to determine  $\alpha_1 P_1$  ( $\alpha_2 P_2$ ) of the top (antitop) quark. The polar angle is defined as the angle between the helicity basis' quantization axis and the final state decay products momentum direction in its parent top quark's rest frame. The

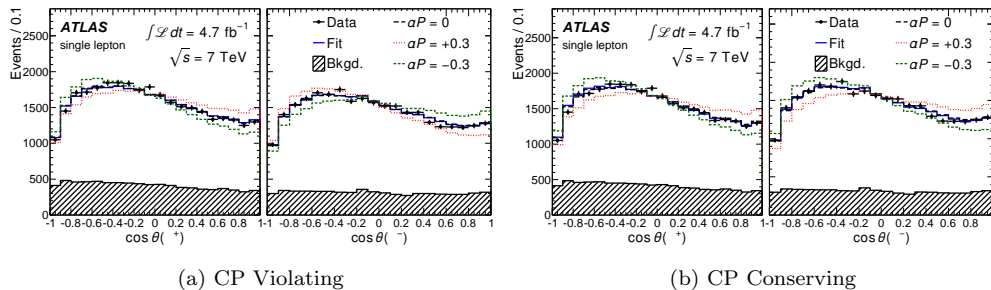


Figure 3: CPC and CPV fits and templates for the single lepton channel.

truth information of each MC signal event is used to reweight the event. After applying the weight, the parton level distributions of the top (antitop) final state decay products, labeled by the index  $i$ , follow the relationship:

$$W(\cos \theta_i) \propto 1 + \alpha_i \cos \theta_i. \quad (4)$$

The value of  $C$  is taken from the signal  $t\bar{t}$  MC (MC@NLO) and is valued at 0.307, with the value of  $\alpha_i P$  chosen as  $\pm 0.3$  to ensure that the cross section in eq. (3) remains positive. Two scenarios for top quark polarization are considered in this analysis: CP conserving (CPC) and CP violating (CPV). The CPC case corresponds to  $\alpha_1 P = \alpha_2 P$ , meanwhile, the CPV case corresponds to  $\alpha_1 P = -\alpha_2 P$ .

Templates of the reconstructed  $\cos \theta_\ell$  are created for the CPC and CPV scenarios, each requiring two sets of templates: a positively polarized and a negatively polarized template. For each scenario, a binned maximum likelihood fit to the data is performed to extract the longitudinal polarization of the top quark. The  $t\bar{t}$  cross section is simultaneously fit to reduce the normalization uncertainty. The fits are performed on all considered channels using charge separated templates. The single lepton result is obtained by multiplying the electron and muon likelihoods together. Similarly, the combined result is obtained by multiplying the single lepton and dilepton channel likelihoods together. The product of the spin-analyzing power and the magnitude of the longitudinal polarization is quoted as the result. Figure 3 shows the CPC and CPV fits and templates.

Templates are created for each source of systematic uncertainty. The systematic uncertainty for the up and down variations is quoted as the mean of the distribution of differences between the central fit value and the systematic template fit to 1,000 pseudo-datasets. The sources of uncertainty that do not depend on the charge of the lepton dramatically reduce the uncertainty in the CPV scenario. This is due to the fit parameters being pushed in opposing directions for the oppositely charged templates. The tension created in the fit leads to the reduced uncertainty.

Table 3 displays the results for  $\alpha_\ell P$  in the single lepton channels. The combined result of the single lepton and dilepton channels for the CPC scenario is

$$\alpha_\ell P_{\text{CPC}} = -0.035 \pm 0.014(\text{stat}) \pm 0.037(\text{syst}) \quad (5)$$

and in the CPV scenario the result is

$$\alpha_\ell P_{\text{CPV}} = 0.020 \pm 0.016(\text{stat})_{-0.017}^{+0.013}(\text{syst}). \quad (6)$$

Table 3: Summary of fitted  $\alpha_\ell P$  in the individual single lepton channels for the CP conserving and CP violating fits. The uncertainties quoted are first statistical and then systematic.

Channel	$\alpha_\ell P_{\text{CPC}}$	$\alpha_\ell P_{\text{CPV}}$
$e$ +jets	$-0.031 \pm 0.028^{+0.043}_{-0.040}$	$0.001 \pm 0.031^{+0.019}_{-0.019}$
$\mu$ +jets	$-0.033 \pm 0.021^{+0.039}_{-0.039}$	$0.036 \pm 0.023^{+0.018}_{-0.017}$
$\ell$ +jets	$-0.034 \pm 0.017^{+0.038}_{-0.037}$	$0.023 \pm 0.019^{+0.012}_{-0.011}$
SM Prediction	0.003 [8]	0.0

 Table 4: Summary of the systematic uncertainties on  $\alpha_\ell P$ . The systematic uncertainties have been added in quadrature to obtain the total systematic uncertainty.

Source	$\Delta\alpha_\ell P_{\text{CPC}}$		$\Delta\alpha_\ell P_{\text{CPV}}$	
Jet reconstruction	+0.031	-0.031	+0.009	-0.005
Lepton reconstruction	+0.006	-0.007	+0.002	-0.001
$E_{\text{T}}^{\text{miss}}$ reconstruction	+0.008	-0.007	+0.004	-0.001
$t\bar{t}$ modeling	+0.015	-0.016	+0.005	-0.013
Background modeling	+0.011	-0.010	+0.005	-0.007
Template statistics	+0.005	-0.005	+0.006	-0.006
Total systematic uncertainty	+0.037	-0.037	+0.013	-0.017

The major sources of uncertainty in the combined result are due to jet energy scale, top mass uncertainty,  $b$ -tagging efficiency, and NP/fake lepton estimation. Table 4 lists the sources of systematic uncertainty for both the CPC and CPV scenarios.

In conclusion, the top quark longitudinal polarization in the CP conserving and CP violating scenarios have been measured and are found to be in agreement with the Standard Model predictions.

## References

- [1] M. L. Mangano, M. Moretti, F. Piccinini, R. Pittau and A. D. Polosa, JHEP **0307** (2003) 001, hep-ph/0206293.
- [2] B. P. Kersevan and E. Richter-Was, hep-ph/0405247.
- [3] M. Aliev, H. Lacker, U. Langenfeld, S. Moch, P. Uwer and M. Wiedermann, Comput. Phys. Commun. **182** (2011) 1034, arXiv:1007.1327 [hep-ph].
- [4] J. M. Butterworth, J. R. Forshaw and M. H. Seymour, Z. Phys. C **72** (1996) 637, hep-ph/9601371.
- [5] G. Corcella, I. G. Knowles, G. Marchesini, S. Moretti, K. Odagiri, P. Richardson, M. H. Seymour and B. R. Webber, JHEP **0101** (2001) 010, hep-ph/0011363.
- [6] H. -L. Lai, M. Guzzi, J. Huston, Z. Li, P. M. Nadolsky, J. Pumplin and C. -P. Yuan, Phys. Rev. D **82** (2010) 074024, arXiv:1007.2241 [hep-ph].
- [7] S. Frixione and B. R. Webber, JHEP **0206** (2002) 029, hep-ph/0204244.
- [8] W. Bernreuther and Z. -G. Si, Physics Letters B **725** (2013) 115, arXiv:1305.2066 [hep-ph].
- [9] V. M. Abazov *et al.* [D0 Collaboration], Phys. Rev. D **84** (2011) 112005, arXiv:1107.4995 [hep-ex].
- [10] V. M. Abazov *et al.* [D0 Collaboration], Phys. Rev. D **87** (2013) 011103, arXiv:1207.0364 [hep-ex].
- [11] T. Aaltonen *et al.* [CDF Collaboration], Phys. Rev. D **87** (2013) 092002, arXiv:1211.1003 [hep-ex].
- [12] S. Fajfer, J. F. Kamenik and B. Melic, JHEP **1208** (2012) 114, arXiv:1205.0264 [hep-ph].

- [13] D. Krohn, T. Liu, J. Shelton and L. -T. Wang, Phys. Rev. D **84** (2011) 074034, arXiv:1105.3743 [hep-ph].
- [14] J. A. Aguilar-Saavedra and M. Perez-Victoria, J. Phys. Conf. Ser. **447** (2013) 012015, arXiv:1302.6618 [hep-ph].
- [15] V. M. Abazov *et al.* [D0 Collaboration], Phys. Rev. D **85** (2012) 091104, arXiv:1201.4156 [hep-ex].
- [16] G. Mahlon and S. J. Parke, Phys. Rev. D **53** (1996) 4886, hep-ph/9512264.
- [17] A. Brandenburg, Z. G. Si and P. Uwer, Phys. Lett. B **539** (2002) 235, hep-ph/0205023.
- [18] G. Aad *et al.* [ATLAS Collaboration], JINST **3** (2008) S08003.
- [19] G. Aad *et al.* [ATLAS Collaboration], arXiv:1307.6511 [hep-ex].
- [20] G. Aad *et al.* [ATLAS Collaboration], Eur. Phys. J. C **72** (2012) 2039, arXiv:1203.4211 [hep-ex].
- [21] G. Aad *et al.* [ATLAS Collaboration], Eur. Phys. J. C **71** (2011) 1577, arXiv:1012.1792 [hep-ex].
- [22] G. Aad *et al.* [ATLAS Collaboration], Eur. Phys. J. C **73** (2013) 2261, arXiv:1207.5644 [hep-ex].
- [23] G. Aad *et al.* [ATLAS Collaboration], Eur. Phys. J. C **72** (2012) 2046, arXiv:1203.5755 [hep-ex].
- [24] W. Bernreuther and Z. -G. Si, Nucl. Phys. B **837** (2010) 90, arXiv:1003.3926 [hep-ph].